*Acta Oceanol. Sin.*, 2022, Vol. 41, No. 4, P. 129–137
https://doi.org/10.1007/s13131-021-1855-6
http://www.aosocean.com
E-mail: ocean2@hyxb.org.cn

# Ocean wave parameters retrieved directly from compact polarimetric SAR data

Yu Liu[1], Yijun He[2]*, Biao Zhang[2]

[1] School of Electronic and Information Engineering, Nanjing University of Information Science & Technology, Nanjing 210044, China

[2] School of Marine Science, Nanjing University of Information Science & Technology, Nanjing 210044, China

Received 25 January 2021; accepted 25 May 2021



**Abstract**

We aim to directly invert wave parameters by using the data of a compact polarimetric synthetic aperture radar (CP SAR) and validate the effectiveness of ocean wave parameter retrieval from the circular transmit/linear receive mode and π/4 compact polarimetric mode. Relevant data from the RADARSAT-2 fully polarimetric SAR on the C-band were used to obtain the compact polarimetric SAR images, and a polarimetric SAR wave retrieval algorithm was used to verify the sea surface wave measurements. Using the data and algorithm, there is no need to estimate complex hydrodynamic modulation transfer functions, even at large radar incidence angles. First, the radar backscattering cross-sections and backscattering cross-section of the radar linearly polarized with any polarization orientation angle were calculated in the two compact polarimetric SAR modes. Then, the wave slopes along the azimuth direction and the range direction were calculated directly using CP SAR data. Finally, we obtained the slope spectrum of the wave from the estimated wave slopes along azimuth and range directions. The wave parameters extracted from the synthetic wave slope spectrum were compared with those obtained from buoy observations of the National Data Buoy Center, verifying a suitable agreement.

**Key words:** RADARSAT-2, CP SAR, wave parameters, wave slope spectrum

**Citation:** Liu Yu, He Yijun, Zhang Biao. 2022. Ocean wave parameters retrieved directly from compact polarimetric SAR data. Acta Oceanologica Sinica, 41(4): 129–137, doi: 10.1007/s13131-021-1855-6

## 1 Introduction

Although fully polarimetric radar systems are being widely used, they present challenges regarding design, antenna technology, data transfer rate, power consumption, and other aspects. Moreover, the fully polarimetric synthetic aperture radar (SAR) mapping width only 1/4 of single polarimetric SAR image with the same other conditions (Souyris et al., 2005; Nord et al., 2009; Collins et al., 2013). To overcome the challenges and disadvantages of fully polarimetric SAR, the compact polarimetric (CP) SAR has attracted research attention in recent years.

The Canadian RADARSAT Constellation Mission launched on June 12, 2019 with three satellites aboard a SpaceX Falcon-9 rocket is jointly conducted by the Canadian Space Agency and the MDA company, which developed a new generation of commercial SAR satellites to replace the RADARSAT-2 satellite from 2007 (Collins et al., 2013; Denbina and Collins, 2012). The new satellite can perform all-weather repeated observations with 90% of the vast area of Canada and 50 m high resolution. As one of the most advanced satellite systems currently available, the SAR satellite of the RADARSAT Constellation Mission provides a multi-polarization mode that includes single linear polarization, bilinear polarization, compact polarization, and four polarization, with the CP mode being its most innovative feature.

Three compact polarization modes have been successively proposed. Souyris et al. (2005) introduced the π/4 CP mode in which the transmitted polarization is linear (Souyris and Mingot, 2002). They also proposed a reconstruction algorithm that may be suitable to reconstruct fully polarimetric data. Stacy and Preiss (2006) proposed a dual circular polarization mode in which the radar system transmits circular polarization waves while receiving left and right circular polarization waves. Although this mode fully leverages the applicability of radar remote sensing in astronomy, it is rarely used in earth observation. Likewise, Raney (2006, 2007) proposed a mixed polarization mode and the corresponding processing method. The system transmits circular polarization waves and receives a set of horizontal and vertical echo signals, establishing a circular transmit/linear receive (CTLR) mode. This mode is simpler and more stable than the dual circular polarization mode, with reduced sensitivity to noise and self-correcting capability. Besides polarization modes, various studies on the mechanism and application of CP SAR have been conducted in topics such as polarization decomposition (Guo et al., 2012; Cloude et al., 2012; Charbonneau et al., 2010), ground object classification (Charbonneau et al., 2010; Chen et al., 2009; Ainsworth et al., 2009), oil spill detection (Shirvany et al., 2012), and glacier detection (Denbina and Collins, 2012). Experimental results have shown that CP SAR data can achieve the applicability of fully polarimetric SAR data.

Along with advance of SAR satellites, the wave inversion algorithm using its data is also continuously improving. Hasselmann and Hasselmann (1991) proposed the method of first guess spectrum, whose calculation result is usually affected by the dif-

Foundation item: The National Natural Science Foundation of China under contract Nos 41620104003 and 42027805; the National Key Research and Development Program under contract No. 2016YFC1401002.
*Corresponding author, E-mail: yjhe@nuist.edu.cn

ference between the initial guess and actual spectrum. Then, they improved the method by dividing the spectrum into a finite independent wave system and adjusting it separately in an iterative process to determine a suitable cost function (Hasselmann et al., 1996). To the solve 180° ambiguity, some wave methods using image cross spectra (Engen and Johnsen, 1995).

Subsequently, He (1999) proposed a parameterized method for wave spectrum inversion mainly based on the SAR image spectrum. In this method, the SAR spectrum of two subimages for inversion should be the same. Mastembroek and Valk (2000) then proposed a semiparametric inversion method without requiring a first guess spectrum to obtain wind wave information through the corresponding scatterometer wind speed and SAR image spectrum. The remaining information of the SAR image spectrum is obtained using a linear relation. Schuler et al. (2002, 2003, 2004) investigated the feasibility of using airborne L- and P-band fully polarimetric SAR data to measure the wave slope and wave spectrum. This method allows direct and effective wave slope measurement. The method was validated using observations of Pacific Ocean surges under low wind. However, this method is only applicable to L- or P-band fully polarimetric SAR data because it should estimate the polarization orientation angle, and the angle generated by C-band data is very noisy.

He et al. (2004) determined the modulation transfer functions of the tilt and polarization orientation angle for linearly polarimetric SAR. Then, He et al. (2006) proposed a method for measuring the wave spectrum using airborne C-band fully polarimetric SAR data. However, this method was only verified by airborne SAR images. Subsequently, Zhang et al. (2010) and He et al. (2009) verified the RADARSAT-2 full-polarization images by using the wave inversion algorithm proposed by He et al. (2006). In 2018, Wang et al. (2018) used Souyris (2005) and Nord (2009) algorithms to reconstruct the pseudo fully polarimetric SAR data from compact polarimetric SAR data, then ocean wave parameters were retrieved from pseudo fully polarimetric SAR data.

In this study, we used C-band RADARSAT-2 data to generate CTLR and π/4 CP SAR images and verify the applicability of a wave information inversion method that extends the proposal by He et al. (2006) to CP SAR images. The wave parameters obtained by the inversion algorithm are verified by the US National Data Buoy Center (NDBC) buoy observations. Section 2 introduces the data collection, in Section 3 introduces the CTLR and π/4 compact polarimetric SAR modes and their wave inversion algorithms. Section 4 analyzes the experimental data and compares the results. Finally, we draw conclusions in Section 5.

## 2 Data sets

We used the four images acquired by the RADARSAT-2 fully polarimetric SAR to verify the direct inversion of wave parameters using CP SAR data. The parameters of a RADARSAT-2 fully polarimetric SAR image are listed in Table 1. The minimum incidence angle is 22.23° and the maximum incidence angle is 24.14°.

The NDBC buoy data for comparison with the inversion wave parameters were obtained from the US National Oceanic and Atmospheric Administration. The data from four buoys were selected. The buoys were approximately located at the center of the SAR image, and their data characteristics are listed in Table 2.

## 3 Theory and methods

### 3.1 *CP SAR*

Wave remote sensing based on CP SAR data is a research hotspot. Problems including whether wave information can be obtained by reconstructing CP SAR data or whether an empirical model can be directly used to build wave information remain to be addressed. Denbina and Collins (2012) used construction polarization data to conduct a glacier target test by constructing pseudo-fully polarimetric SAR data, achieving promising results. Yin et al. (2011) obtained the covariance matrix by using a modified reconstruction model to suitably describe the characteristics of maritime objects such as ships. Wang et al. (2018) used the Souyris et al. (2005) and Nord et al. (2009) algorithms to reconstruct fully polarimetric SAR data from CP SAR data. They evaluated both the reconstruction ability of the two algorithms and wave parameter inversion using the CP SAR data.

CP SAR transmits a single polarization (e.g., linear horizontal or right circular) and performs reception along two orthogonal polarizations, thus reducing the system complexity regarding design and maintenance and expanding the imaging range. There are three main CP modes: π/4, dual circular polarization, and CTLR. We focused on the CTLR and π/4 modes in this study.

#### 3.1.1 *CTLR mode*

In the CTLR mode, the right circular polarization electromagnetic waves are emitted, and the horizontal and vertical electromagnetic waves are received to obtain the compact polarimetric SAR data.

When the system transmits the right circular polarization electromagnetic wave, the received backscatter vector can be expressed as:

**Table 1.** RADARSAT-2 fully polarimetric data parameters for SAR image acquired on February 25, 2009

| Parameter | Value |
|---|---|
| Radar center frequency/GHz | 5.40 |
| Processing facility | GSS |
| Raw data start time | 2009-01-11To2:25:04.232940Z |
| Satellite height/km | 798.0 |
| Track angle/(°) | 17.54 |
| Sampled pixel spacing/m | 4.7 |
| Sampled line spacing/m | 4.9 |
| Minimum incidence angle/(°) | 22.23 |
| Maximum incidence angle/(°) | 24.14 |

**Table 2.** RADARSAT-2 fully polarimetric synthetic aperture radar image data and National Data Buoy Center buoy information

| Image ID | Acquired time (UTC) | Buoy time | Image central site | Buoy site | Wind speed/(m·s$^{-1}$) | Wind direction/(°) |
|---|---|---|---|---|---|---|
| 1 | 02:25:04<br>Jan. 11, 2009 | 02:50:00<br>Jan. 11, 2009 | 46°04′00″N,<br>131°02′22″W | 46°03′00″N,<br>131°01′12″W | 9.0 | 240 |
| 2 | 02:09:26<br>Feb. 25, 2009 | 01:50:00<br>Feb. 19, 2009 | 35°44′43″N,<br>121°55′42″W | 35°44′29″N,<br>121°53′03″W | 5.3 | 321 |
| 3 | 14:30:58<br>Jan. 18, 2009 | 14:50:00<br>Jan. 18, 2009 | 45°57′43″N,<br>125°39′18″W | 45°54′28″N,<br>125°45′37″W | 3.7 | 97 |
| 4 | 05:47:58<br>Feb. 28, 2009 | 05:50:00<br>Feb. 28, 2009 | 51°07′18″N,<br>178°53′10″W | 51°09′17″N,<br>179°00′02″W | 4.0 | 270 |

$$\Lambda_{\mathrm{B\_CTLR}} = \boldsymbol{S} \times \boldsymbol{J} = \frac{1}{\sqrt{2}} \begin{bmatrix} \boldsymbol{S}_{\mathrm{HH}} - \mathrm{i}\boldsymbol{S}_{\mathrm{HV}} \\ \boldsymbol{S}_{\mathrm{HV}} - \mathrm{i}\boldsymbol{S}_{\mathrm{VV}} \end{bmatrix}, \tag{1}$$

where $\boldsymbol{S}$ represents the scattering matrix of the fully polarimetric SAR; $\boldsymbol{J}$ represents the Jones vector of the polarized electromagnetic wave; $\boldsymbol{S}_{pq}$ represents the complex scattering coefficient in the four-polarization SAR, $p$ represents the polarization mode of the electromagnetic wave emitted by the radar, and $q$ represents the polarization mode of the electromagnetic wave received by the radar; $\boldsymbol{S}_{\mathrm{HH}}$, $\boldsymbol{S}_{\mathrm{VV}}$ and $\boldsymbol{S}_{\mathrm{HV}}$ represents the scattering matrix elements of horizonal, vertical and cross channels, respectively; $i$ is the imaginary unit.

The vertical and horizontal echo signals received by the radar are respectively expressed as

$$\boldsymbol{S}_{\mathrm{RH}} = \boldsymbol{J}_{\mathrm{V}}^{t} \Lambda_{\mathrm{B\_CTLR}} = \frac{1}{\sqrt{2}} \begin{bmatrix} 0 & 1 \end{bmatrix} \begin{bmatrix} \boldsymbol{S}_{\mathrm{HH}} - \mathrm{i}\boldsymbol{S}_{\mathrm{HV}} \\ \boldsymbol{S}_{\mathrm{HV}} - \mathrm{i}\boldsymbol{S}_{\mathrm{VV}} \end{bmatrix} = \frac{1}{\sqrt{2}} \begin{bmatrix} \boldsymbol{S}_{\mathrm{HV}} - \mathrm{i}\boldsymbol{S}_{\mathrm{VV}} \end{bmatrix}, \tag{2}$$

$$\boldsymbol{S}_{\mathrm{RV}} = \boldsymbol{J}_{\mathrm{H}}^{t} \Lambda_{\mathrm{B\_CTLR}} = \frac{1}{\sqrt{2}} \begin{bmatrix} 1 & 0 \end{bmatrix} \begin{bmatrix} \boldsymbol{S}_{\mathrm{HH}} - \mathrm{i}\boldsymbol{S}_{\mathrm{HV}} \\ \boldsymbol{S}_{\mathrm{HV}} - \mathrm{i}\boldsymbol{S}_{\mathrm{VV}} \end{bmatrix} = \frac{1}{\sqrt{2}} \begin{bmatrix} \boldsymbol{S}_{\mathrm{HH}} - \mathrm{i}\boldsymbol{S}_{\mathrm{HV}} \end{bmatrix}, \tag{3}$$

where $\boldsymbol{J}_{\mathrm{V}}^{t}$ represents the Jones vector of vertically polarized electromagnetic waves per unit time; $\boldsymbol{J}_{\mathrm{H}}^{t}$ represents the Jones vector of horizontally polarized electromagnetic waves per unit time; $\boldsymbol{S}_{\mathrm{RH}}$ and $\boldsymbol{S}_{\mathrm{RV}}$ represent the complex scattering coefficient of RH polarization in CTLR mode, and the complex scattering coefficient of RV polarization in CTLR mode, respectively.

The backward scattering coefficient of electromagnetic wave is given by

$$\vec{k}_{\mathrm{CTLR}} = \frac{1}{\sqrt{2}} \begin{bmatrix} \boldsymbol{S}_{\mathrm{RH}} \\ \boldsymbol{S}_{\mathrm{RV}} \end{bmatrix} = \frac{1}{\sqrt{2}} \begin{bmatrix} \boldsymbol{S}_{\mathrm{HH}} - \mathrm{i}\boldsymbol{S}_{\mathrm{HV}} \\ \boldsymbol{S}_{\mathrm{HV}} - \mathrm{i}\boldsymbol{S}_{\mathrm{VV}} \end{bmatrix}. \tag{4}$$

The covariance matrix of the CTLR mode is given by

$$\begin{aligned} C_{\mathrm{CTLR}} &= \left\langle \vec{k}_{\mathrm{CTLR}} \cdot \vec{k}^{*}{}_{\mathrm{CTLR}} \right\rangle \\ &= \frac{1}{2} \begin{bmatrix} \left\langle |\boldsymbol{S}_{\mathrm{HH}}|^2 \right\rangle & \langle \mathrm{i}\,(\boldsymbol{S}_{\mathrm{HH}} \cdot \boldsymbol{S}_{\mathrm{VV}}^{*}) \rangle \\ \langle -\mathrm{i}\,(\boldsymbol{S}_{\mathrm{VV}} \cdot \boldsymbol{S}_{\mathrm{HH}}^{*}) \rangle & \left\langle |\boldsymbol{S}_{\mathrm{VV}}|^2 \right\rangle \end{bmatrix} + \\ &\quad \frac{1}{2} \begin{bmatrix} \left\langle |\boldsymbol{S}_{\mathrm{HV}}|^2 \right\rangle & \left\langle -\mathrm{i}|\boldsymbol{S}_{\mathrm{HV}}|^2 \right\rangle \\ \left\langle \mathrm{i}|\boldsymbol{S}_{\mathrm{HV}}|^2 \right\rangle & \left\langle |\boldsymbol{S}_{\mathrm{HV}}|^2 \right\rangle \end{bmatrix} + \\ &\quad \frac{1}{2} \begin{bmatrix} -2\Re\left(\langle \boldsymbol{S}_{\mathrm{HH}} \cdot \boldsymbol{S}_{\mathrm{HV}}^{*} \rangle\right) & \langle \boldsymbol{S}_{\mathrm{HH}} \cdot \boldsymbol{S}_{\mathrm{HV}}^{*} \rangle + \langle \boldsymbol{S}_{\mathrm{HV}} \cdot \boldsymbol{S}_{\mathrm{VV}}^{*} \rangle \\ \langle \boldsymbol{S}_{\mathrm{HV}} \cdot \boldsymbol{S}_{\mathrm{HH}}^{*} \rangle + \langle \boldsymbol{S}_{\mathrm{VV}} \cdot \boldsymbol{S}_{\mathrm{HV}}^{*} \rangle & 2\Re\left(\langle \boldsymbol{S}_{\mathrm{VV}} \cdot \boldsymbol{S}_{\mathrm{HV}}^{*} \rangle\right) \end{bmatrix}, \end{aligned} \tag{5}$$

where $\Re$ represents the real part of the complex scattering coefficient, $\langle \cdot \rangle$ means average the matrix, * denotes matrix conjugate. Considering the reflection symmetry, the CTLR covariance matrix can be simplified as follows:

$$\begin{aligned} C_{\mathrm{CTLR}} &= \left\langle \vec{k}_{\mathrm{CTLR}} \cdot \vec{k}^{*}{}_{\mathrm{CTLR}} \right\rangle \\ &= \frac{1}{2} \begin{bmatrix} \left\langle |\boldsymbol{S}_{\mathrm{HH}}|^2 \right\rangle & \langle \mathrm{i}\,(\boldsymbol{S}_{\mathrm{HH}} \cdot \boldsymbol{S}_{\mathrm{VV}}^{*}) \rangle \\ \langle -\mathrm{i}\,(\boldsymbol{S}_{\mathrm{VV}} \cdot \boldsymbol{S}_{\mathrm{HH}}^{*}) \rangle & \left\langle |\boldsymbol{S}_{\mathrm{VV}}|^2 \right\rangle \end{bmatrix} + \\ &\quad \frac{1}{2} \begin{bmatrix} \left\langle |\boldsymbol{S}_{\mathrm{HV}}|^2 \right\rangle & \left\langle -\mathrm{i}|\boldsymbol{S}_{\mathrm{HV}}|^2 \right\rangle \\ \left\langle \mathrm{i}|\boldsymbol{S}_{\mathrm{HV}}|^2 \right\rangle & \left\langle |\boldsymbol{S}_{\mathrm{HV}}|^2 \right\rangle \end{bmatrix}. \end{aligned} \tag{6}$$

#### 3.1.2 *π/4 mode*

In the π/4 mode transmits 45° linearly polarized electromagnetic waves and receives both horizontal and vertical electromagnetic waves. The received backscatter vector can be expressed as

$$\Lambda_{\mathrm{B\_}\pi/4} = \frac{1}{\sqrt{2}} \begin{bmatrix} \boldsymbol{S}_{\mathrm{HH}} + \boldsymbol{S}_{\mathrm{HV}} \\ \boldsymbol{S}_{\mathrm{VV}} + \boldsymbol{S}_{\mathrm{HV}} \end{bmatrix}. \tag{7}$$

The vertical and horizontal echo signals received by the radar can be expressed as

$$\boldsymbol{S}_{\mathrm{VV}} = \boldsymbol{J}_{\mathrm{V}}^{t} \Lambda_{\mathrm{B\_}\pi/4} = \frac{1}{\sqrt{2}} \begin{bmatrix} 0 & 1 \end{bmatrix} \begin{bmatrix} \boldsymbol{S}_{\mathrm{HH}} + \boldsymbol{S}_{\mathrm{HV}} \\ \boldsymbol{S}_{\mathrm{VV}} + \boldsymbol{S}_{\mathrm{HV}} \end{bmatrix} = \frac{1}{\sqrt{2}} \begin{bmatrix} \boldsymbol{S}_{\mathrm{VV}} + \boldsymbol{S}_{\mathrm{HV}} \end{bmatrix}, \tag{8}$$

$$\boldsymbol{S}_{\mathrm{HH}} = \boldsymbol{J}_{\mathrm{H}}^{t} \Lambda_{\mathrm{B\_}\pi/4} = \frac{1}{\sqrt{2}} \begin{bmatrix} 1 & 0 \end{bmatrix} \begin{bmatrix} \boldsymbol{S}_{\mathrm{HH}} + \boldsymbol{S}_{\mathrm{HV}} \\ \boldsymbol{S}_{\mathrm{VV}} + \boldsymbol{S}_{\mathrm{HV}} \end{bmatrix} = \frac{1}{\sqrt{2}} \begin{bmatrix} \boldsymbol{S}_{\mathrm{HH}} + \boldsymbol{S}_{\mathrm{HV}} \end{bmatrix}. \tag{9}$$

The backward scattering coefficient of electromagnetic wave is given by

$$\vec{k}_{\pi/4} = \frac{1}{\sqrt{2}} \begin{bmatrix} \boldsymbol{S}_{\mathrm{HH}} + \boldsymbol{S}_{\mathrm{HV}} \\ \boldsymbol{S}_{\mathrm{VV}} + \boldsymbol{S}_{\mathrm{HV}} \end{bmatrix}. \tag{10}$$

The covariance matrix of the π/4 mode is given by

$$\begin{aligned} \boldsymbol{C}_{\pi/4} = \left\langle \vec{k}^{*}{}_{\pi/4} \cdot \vec{k}_{\pi/4} \right\rangle &= \frac{1}{2} \begin{bmatrix} \left\langle |\boldsymbol{S}_{\mathrm{HV}}|^2 \right\rangle & \left\langle |\boldsymbol{S}_{\mathrm{HV}}|^2 \right\rangle \\ \left\langle |\boldsymbol{S}_{\mathrm{HV}}|^2 \right\rangle & \left\langle |\boldsymbol{S}_{\mathrm{HV}}|^2 \right\rangle \end{bmatrix} + \\ &\quad \frac{1}{2} \begin{bmatrix} \left\langle |\boldsymbol{S}_{\mathrm{HH}}|^2 \right\rangle & \langle \boldsymbol{S}_{\mathrm{HH}} \cdot \boldsymbol{S}_{\mathrm{VV}}^{*} \rangle \\ \langle \boldsymbol{S}_{\mathrm{VV}} \cdot \boldsymbol{S}_{\mathrm{HH}}^{*} \rangle & \left\langle |\boldsymbol{S}_{\mathrm{VV}}|^2 \right\rangle \end{bmatrix} + \\ &\quad \frac{1}{2} \begin{bmatrix} 2\Re\left(\langle \boldsymbol{S}_{\mathrm{HH}} \cdot \boldsymbol{S}_{\mathrm{HV}}^{*} \rangle\right) & \langle \boldsymbol{S}_{\mathrm{HH}} \cdot \boldsymbol{S}_{\mathrm{HV}}^{*} \rangle + \langle \boldsymbol{S}_{\mathrm{VV}}^{*} \cdot \boldsymbol{S}_{\mathrm{HV}} \rangle \\ \langle \boldsymbol{S}_{\mathrm{VV}} \cdot \boldsymbol{S}_{\mathrm{HV}}^{*} \rangle + \langle \boldsymbol{S}_{\mathrm{HH}}^{*} \cdot \boldsymbol{S}_{\mathrm{HV}} \rangle & 2\Re\left(\langle \boldsymbol{S}_{\mathrm{VV}} \cdot \boldsymbol{S}_{\mathrm{HV}}^{*} \rangle\right) \end{bmatrix}. \end{aligned} \tag{11}$$

Similarly, according to the reflection symmetry, the π/4 covariance matrix can be simplified as

$$\begin{aligned} \boldsymbol{C}_{\pi/4} = \left\langle \vec{k}_{\pi/4} \cdot \vec{k}^{*}{}_{\pi/4} \right\rangle &= \frac{1}{2} \begin{bmatrix} \left\langle |\boldsymbol{S}_{\mathrm{HV}}|^2 \right\rangle & \left\langle |\boldsymbol{S}_{\mathrm{HV}}|^2 \right\rangle \\ \left\langle |\boldsymbol{S}_{\mathrm{HV}}|^2 \right\rangle & \left\langle |\boldsymbol{S}_{\mathrm{HV}}|^2 \right\rangle \end{bmatrix} + \\ &\quad \frac{1}{2} \begin{bmatrix} \left\langle |\boldsymbol{S}_{\mathrm{HH}}|^2 \right\rangle & \langle \boldsymbol{S}_{\mathrm{HH}} \cdot \boldsymbol{S}_{\mathrm{VV}}^{*} \rangle \\ \langle \boldsymbol{S}_{\mathrm{VV}} \cdot \boldsymbol{S}_{\mathrm{HH}}^{*} \rangle & \left\langle |\boldsymbol{S}_{\mathrm{VV}}|^2 \right\rangle \end{bmatrix}. \end{aligned} \tag{12}$$

In this paper, based on the relationship between the compact polarization and the full polarization scattering matrix, the inversion of the wave parameters by the CTLR and π/4 compact polarization models are mainly verified.

### 3.2 *Wave spectrum retrieval algorithm*

As linear polarization contributes the most to the wave slope, we assume that the ellipticity is zero. Thus, the backscattering cross-section at any polarization orientation can be derived as follows (Schuler et al., 2004; He et al., 2006):

$$\sigma(0,\psi)=\frac{1}{4}(\sigma_{HH}+\sigma_{VV})\left[1+\cos^2(2\psi)\right]+\frac{1}{2}(\sigma_{HH}-\sigma_{VV})\cos 2\psi+\sigma_{HV}+\frac{1}{2}\Re(\sigma_{HHVV})\sin^2(2\psi), \tag{13}$$

where $\sigma_{HH}$, $\sigma_{VV}$ and $\sigma_{HV}$ represent the horizontal, vertical and cross polarization of the line-polarized backscattering cross section respectively. $\sigma_{HHVV}$ can be derived directly from the covariance matrix of the CTLR model to represent the correlation relationship between horizontal and vertical polarization.

Under the background of linear modulation, real aperture radar is used to detect the change between sea surface height and local backscattering cross section. They can represent superpositions of wave numbers of $k$ and frequency of $\omega$. The corresponding relation is given by

$$\xi(\boldsymbol{r},t)=\sum_k \xi_k \exp\left[\mathrm{i}(k\cdot\boldsymbol{r}-\omega t)\right]+c.c, \tag{14}$$

$$\sigma_{PP}(\boldsymbol{r},t)=\overline{\sigma_{PP}}\left(1+\left\{\sum_k \xi_k T^R_{PPK}\exp\left[\mathrm{i}(k\cdot\boldsymbol{r}-\omega t)\right]+c.c\right\}\right), \tag{15}$$

where $\xi$ is sea level, $k$ is the wave number, $\boldsymbol{r}$ is the wave space vector, $\omega$ is the angular frequency of the wave, and $c.c$ is the conjugate complex of the series. $\xi_k$ for Fourier coefficient $\xi(\boldsymbol{r},t)$. Subscript pp said radar emission polarization and receive, in which $p$ = H, V, $\psi$ are horizontal polarization, vertical polarization and linear polarization with polarization orientation angle given by $\psi$. $T^R_{PPK}$ represents the real synthetic aperture radar (RAR) modulation transfer function, which includes tilt modulation (Fung and Chen, 1969), hydrodynamic modulation (Valenzuela, 1978), polarization orientation angle modulation (Lee et al., 2000; Lee et al., 2002), and shift modulation along the range and azimuth directions.

For a SAR, a velocity bunching modulation must be included. In all the modulation terms, only the modulation transfer functions of the tilt and polarization orientation angle depend on the radar polarization. Moreover, the wave slope generated by the polarization orientation angle can be ignored for the horizontal and vertical polarizations (He et al., 2004). There are no polarization-sensitive terms for hydrodynamic modulation, velocity bunching, and range and azimuthal directional shift modulation. Therefore, Eq. (15) can be simplified as follows:

$$\frac{\Delta\sigma_{VV}(\boldsymbol{r},t)}{\overline{\sigma_{VV}}}-\frac{\Delta\sigma_{HH}(\boldsymbol{r},t)}{\overline{\sigma_{HH}}}=\sum_k \xi_k(T^t_{kVV}-T^t_{kHH})\exp\left[\mathrm{i}(k\cdot\boldsymbol{r}-\omega t)\right]+c_1, \tag{16a}$$

$$\frac{\Delta\sigma_{\psi\psi}(\boldsymbol{r},t)}{\overline{\sigma_{\psi\psi}}}-\frac{\Delta\sigma_{VV}(\boldsymbol{r},t)}{\overline{\sigma_{VV}}}=\sum_k \xi_k(T^t_{k\psi\psi}+T^p_{k\psi\psi}-T^t_{kVV})\exp[\mathrm{i}(k\cdot\boldsymbol{r}-\omega t)]+c_2, \tag{16b}$$

where $c_1$ and $c_2$ are the complex conjugate of the series, respectively, $T^p_{k\psi\psi}$ and $T^t_{k\psi\psi}$ are given by He et al. (2004), and for VV polarization ($\psi=\pi/8$) and HH polarization ($\psi=\pi/8$), we can obtain

$$T^t_{kVV}=\mathrm{i}k_x\frac{4-0.5(1-\sin^2\theta)}{\tan\theta(1-\sin^2\theta)}, \tag{17a}$$

$$T^t_{kHH}=\mathrm{i}k_x\frac{4-0.5(1+\sin^2\theta)}{\tan\theta(1+\sin^2\theta)}. \tag{17b}$$

By substituting Eqs (17a) and (17b) (Eqs (15a) and (15b) in He et al. (2004)) into Eq. (16), we can obtain

$$\frac{\Delta\sigma_{VV}}{\overline{\Delta\sigma_{VV}}}-\frac{\Delta\sigma_{HH}}{\overline{\Delta\sigma_{HH}}}=-\frac{8\tan\theta}{1+\sin^2\theta}\frac{\partial\xi}{\partial x}, \tag{18a}$$

$$\frac{\Delta\sigma_{\psi\psi}}{\overline{\sigma_{\psi\psi}}}-\frac{\Delta\sigma_{VV}}{\overline{\Delta\sigma_{VV}}}=A\frac{\partial\xi}{\partial x}+B\frac{\partial\xi}{\partial y}, \tag{18b}$$

where $\frac{\partial\xi}{\partial x}$, $\frac{\partial\xi}{\partial y}$ represent the wave slopes in the direction of range and azimuth, respectively. Parameters $A$ and $B$ are given by Eq. (8) of He et al. (2006).

According to the linearly polarized wave inversion detailed above, we use the relation between the CTLR mode and scattering matrix to establish a new formulation and the CTLR mode to further verify the wave inversion algorithm. The new formulation of the linearly polarized backscattering cross-section at any polarization angle is given by

$$\sigma_{CTLR}(0,\psi)=\frac{1}{2}(\mathrm{CTLR11}+\mathrm{CTLR22})\left[1+\cos^2(2\psi)\right]+(\mathrm{CTLR11}-\mathrm{CTLR22})\cos 2\psi+\frac{1}{2}\left[\Re(\mathrm{CTLR21}-\mathrm{CTLR12})+\sigma_{HV}\right]\sin^2(2\psi), \tag{19}$$

where CTLR11, CTLR22, CTLR12, and CTLR21 represent the scattering matrix elements of CTLR mode, and replace $\sigma_{HH}$, $\sigma_{VV}$ and $\sigma_{HV}$ of full-polarization mode.

To improve the experimental results, after a feasibility analysis of the equation, we set $\psi$=π/8 for verification. Similarly, a new polarization relationship can be derived from Eqs (18a) and (18b):

$$\frac{\Delta\mathrm{CTLR22}}{\overline{\mathrm{CTLR22}}}-\frac{\Delta\mathrm{CTLR11}}{\overline{\mathrm{CTLR11}}}=-\frac{8\tan\theta}{1+\sin^2\theta}\frac{\partial\xi}{\partial x}, \tag{20a}$$

$$\frac{\Delta\sigma_{\psi\psi}}{\overline{\sigma_{\psi\psi}}}-\frac{\Delta\mathrm{CTLR22}}{\overline{\mathrm{CTLR22}}}=A\frac{\partial\xi}{\partial x}+B\frac{\partial\xi}{\partial y}, \tag{20b}$$

where $\sigma_{\psi\psi}$ denotes the radar backscattering cross sections at polarization orientation angle $\psi$, the subscript $\psi=\pi/8$. The other parameters, $A$ and $B$ are consistent with Eqs (18a) and (18b). In this approach, cross-polarization information is not directly used in calculating the backscattering cross section of linear polarization. Here, co-polarization and cross-polarization measurements are directly used to estimate the backscattering cross section of linear polarization and to invert the wave slope and spectrum. The specific steps of wave information extraction are as follows:

(1) Select 512×512 pixel size CTLR (RH, RV) polarization images.

(2) Calculate linearly polarized image by using Eq. (19) for polarization angle $\psi=\pi/8$.

(3) Use Eqs (20a) and (20b) to calculate the slope of the sea surface and a 3 × 3 Gaussian filter to smooth the slope images.

(4) The wave slope spectrum is obtained to calculate the wavelength, significant wave height, wave period and corresponding wave spectrum.

As the π/4 mode adopts the same method as the CTLR mode and similar equations and experimental verification, we omit its details for brevity.

## 4 Results and analysis

In this paper, four RADARSAT-2 C-band full polarimetric SAR images are used to simulate the two modes: CTLR mode and π/4 mode, and the wave parameters, the wave slope and wave spectrum are both retrieved from CTLR and π/4 images. The information of CP SAR images and buoy data acquisition are described in Table 2. A total of four buoy data are used in this experiment. Due to the need for quantitative comparison of inversion parameters and buoy data, the buoys were all located at the center of SAR image, and the RADARSAT-2 observation time and buoy measurements time interval are all less than 30 min.

Figures 1 and 2 show the vertical polarization CP SAR image

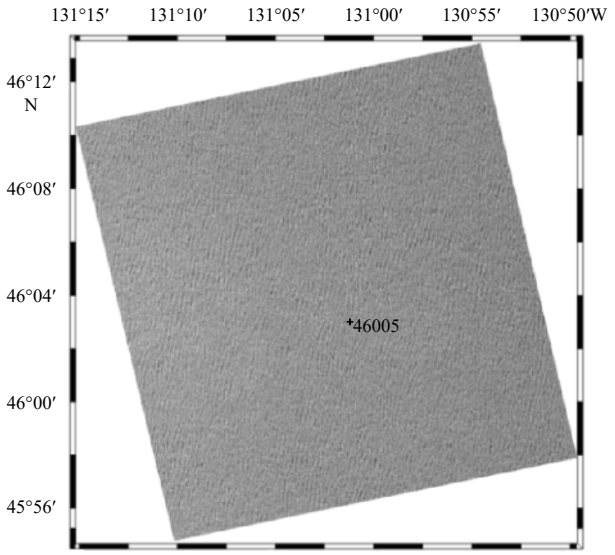


**Fig. 1.** A C band vertically polarized, image of area west of Aberdeen, WA acquired by RADARSAT-2 at 02:25 UTC on January 11, 2009. RADARSAT-2 Data and Products© MacDonald, Dettwiler and Associates Ltd. (2008–2009)-ALL Rights Reserved.

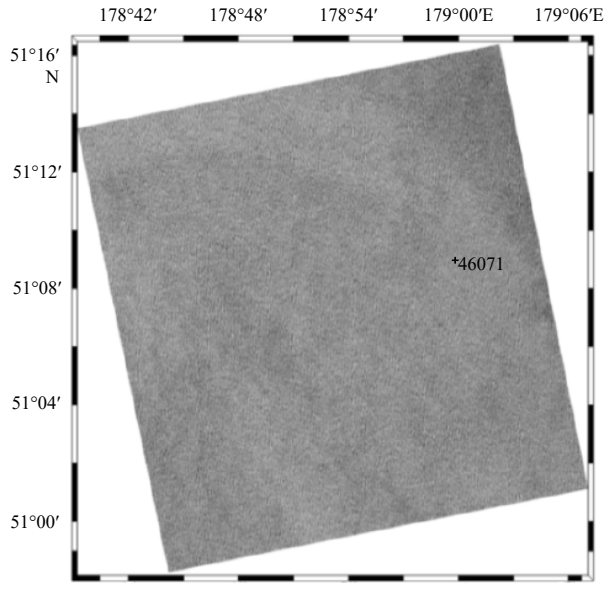


**Fig. 2.** A C band vertically polarized, image of area south of Amchitkais, AK acquired by RADARSAT-2 at 05:47 UTC on February 28, 2009. RADARSAT-2 Data and Products© MacDonald, Dettwiler and Associates Ltd. (2008–2009)-ALL Rights Reserved.

obtained by CTLR mode of an area west of Aberdeen, WA and an area south of Amchitkais, AK, respectively. Corresponding 512 × 512 pixel size horizontally (RH) and vertically (RV) polarized images selected from these CP SAR images are presented in Figs 3a, 3b, 4a and 4b, respectively. Figures 3c and 4c represents the corresponding 512×512 pixel size line-polarized images, which are derived from the RH and RV images, and the polarization orientation angle ($\psi = \pi/8.$). The obtained wave range and azimuth directions images are respectively shown in Figs 3d, 3e, 4d and 4e. Then 3×3 Gaussian filter was used to smooth the slope images. Finally, Figs 5 and 6 represents the retrieved wave spectrum, from which we can extract the corresponding wavelengths, significant wave heights and wave directions.

During retrieval of wave information, no external information was obtained by guessing the wave spectrum using a wave model or observing the wind provided by the scatterometer, resulting in a 180° direction ambiguity. We used the direction of the wave as measured by the buoy and the direction of the wind to eliminate this ambiguity. In Figs 5 and 6, it can be concluded that the dominant wavelengths are 405.4 m and 202.7 m, respectively, and the dominant wave propagation directions are 271.4° and 273.6°, respectively. The collocated NDBC (46005, 46071) buoy-measured the dominant wavelengths are 399.5 m and 188.8 m, respectively, and dominant wave propagation directions are 240° and 270°, respectively.

Similarly, four RADARSAT-2 fully polarimetric images on the C-band were used to simulate the π/4 mode. Figures 7 and 8 show the vertical polarization CP SAR image with the π/4 mode of the west of Aberdeen, WA and south of Amchitkais, AK, respectively. From the wave spectrum in Figs 7 and 8, the dominant wavelengths are 418.9 m and 203.3 m, respectively, and the dominant wave propagation directions are 271.2° and 274.0°, respectively.

In our study, the results also show that the wave parameters retrieved from the two modes are in a good agreement with those from NDBC buoys (46028, 46089).

Waves traveling at arbitrary propagation angles can be handled by considering measurement pairs along orthogonal directions, as determined by the satellite flight path. To extract wave parameters, we can refer to the following equations. First, we can estimate the root-mean-square slope of the propagation direction $S_{\mathrm{rms}}$ and the wave propagation direction $\Phi$:

$$S_{\mathrm{rms}} = \left[\left(\langle S_{\mathrm{r}}\cos\Phi\rangle\right)^2 + \left(\langle S_{\mathrm{a}}\sin\Phi\rangle\right)^2\right]^{1/2}, \tag{21}$$

where $S_{\mathrm{r}} = \dfrac{\partial\xi}{\partial x}$ and $S_{\mathrm{a}} = \dfrac{\partial\xi}{\partial y}$ are the wave slopes in the range and azimuth directions; and $\Phi$ is the wave propagation direction (north is 0°, clockwise rotation, east is 90°). Moreover, the dominant wave height is obtained by using the relation between $S_{\mathrm{rms}}$ and dominant wavelength $\lambda_{\mathrm{d}}$:

$$\tan\left(S_{\mathrm{rms}}\right) = H_{\mathrm{d}}/(\lambda_{\mathrm{d}}/2). \tag{22}$$

Table 3 shows that wave parameters, which are wave period, wavelength, wave direction, significant wave height and root-mean-square slope, retrieved from CP SAR data are compared with these measured by the buoys. The inverse wave parameters obtained from the CP SAR data are consistent with those obtained from the buoy measurements. Thus, the proposed calculation method can retrieve wave parameters from CP SAR images. As the wave slope spectrum obtained by inversion is a combina-

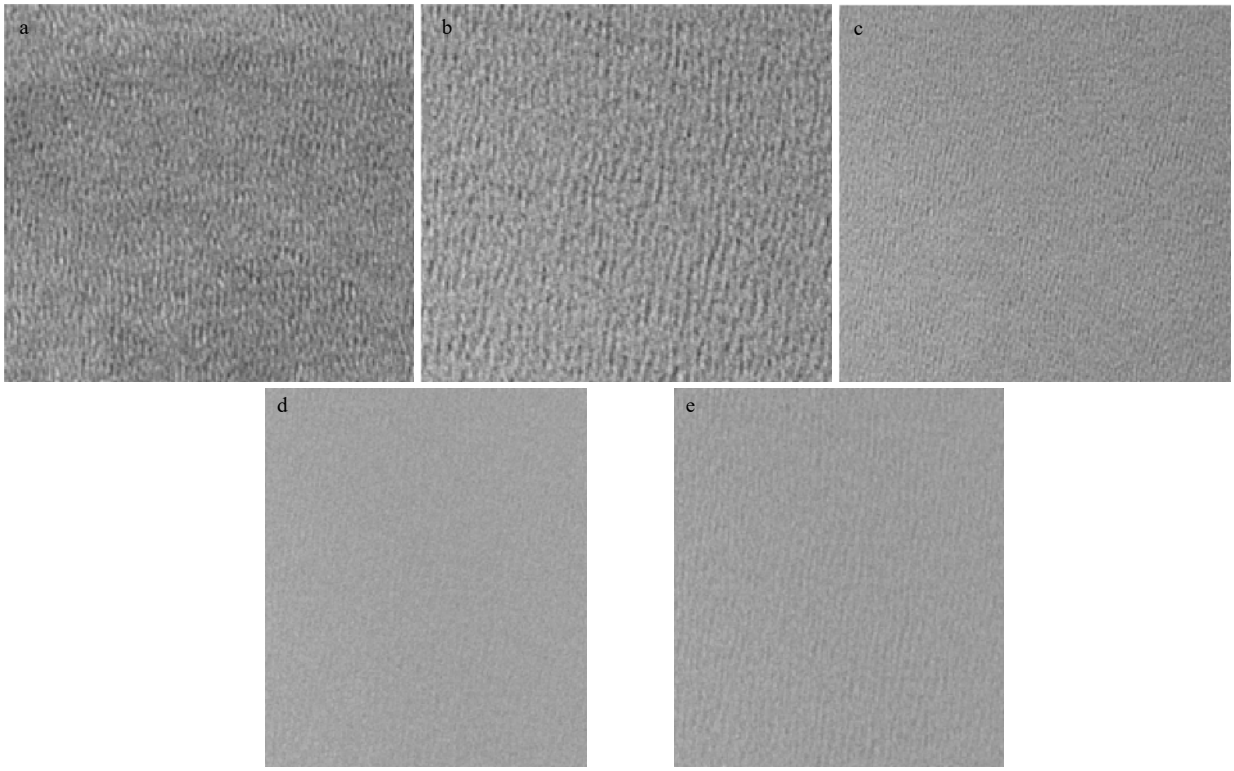


**Fig. 3.** Corresponding 512×512 pixel size images of area west of Aberdeen, WA acquired by RADARSAT-2 at 02:25 UTC on January 11, 2009, showing horizontal polarization (a), vertical polarization (b), linear polarization (c), wave slope image in the range direction (d), and wave slope image in the azimuth direction (e). NDBC directional wave buoy (46005) is collocated to these images.

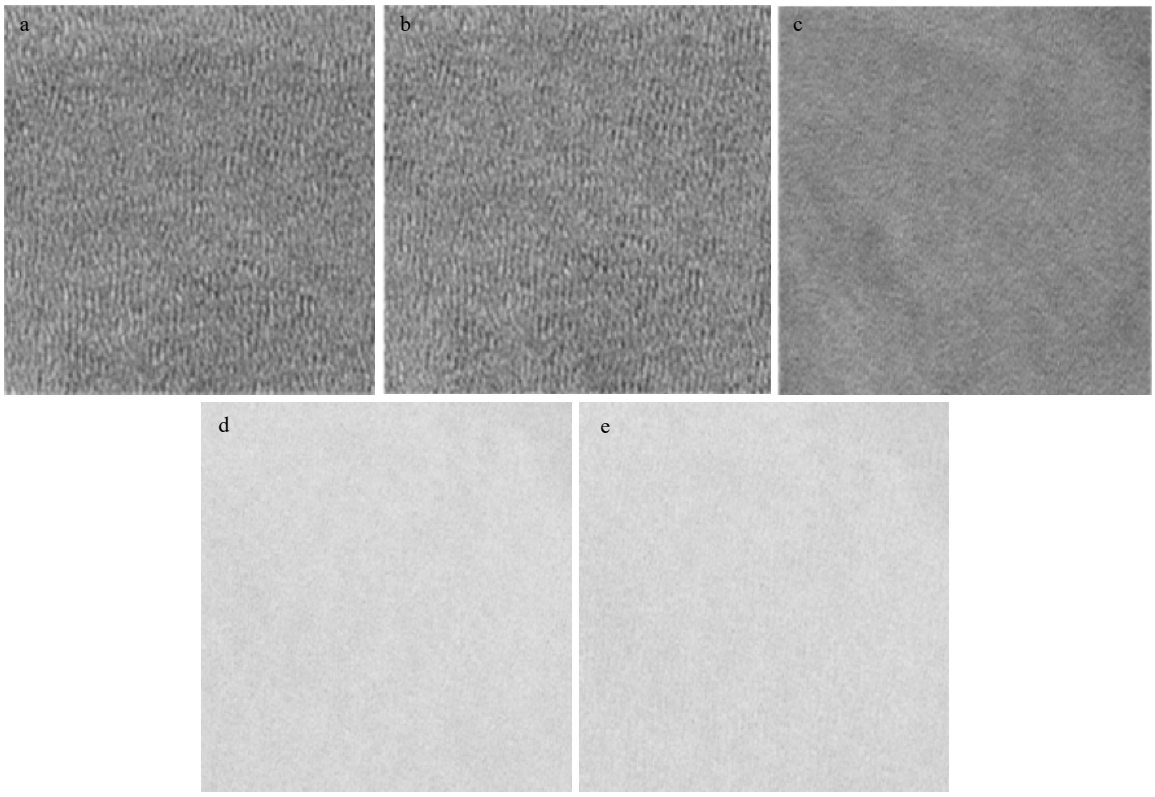


**Fig. 4.** Corresponding 512×512 pixel size images of area south of Amchitkais, AK acquired by RADARSAT-2 at 05:47 UTC on February 28, 2009, showing horizontal polarization (a), vertical polarization (b), linear polarization (c), wave slope image in the range direction (d), and wave slope image in the azimuth direction (e). NDBC directional wave buoy (46071) is collocated to these images.

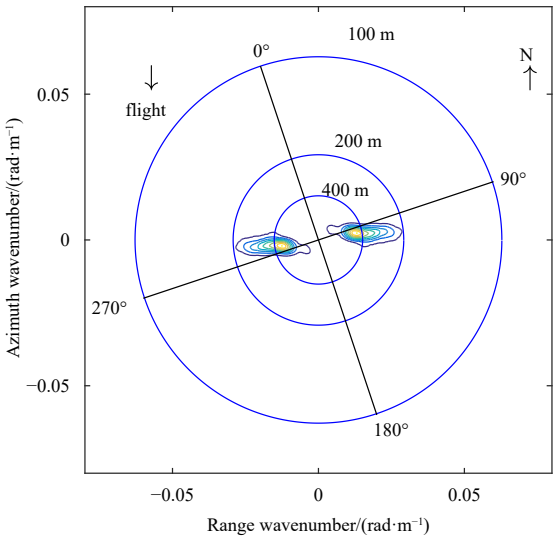


**Fig. 5.** Wave slope spectrum image obtained by CTLR mode of area west of Aberdeen, WA acquired by RADARSAT-2 at 02:25 UTC on January 11, 2009.

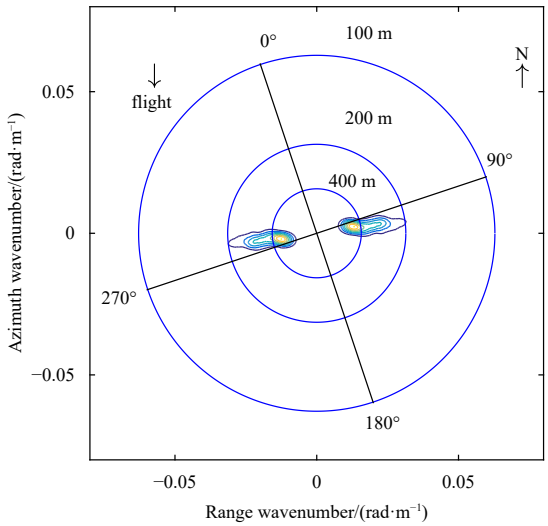


**Fig. 7.** Wave slope spectrum image obtained by π/4 mode of area west of Aberdeen, WA acquired by RADARSAT-2 at 02:25 UTC on January 11, 2009.

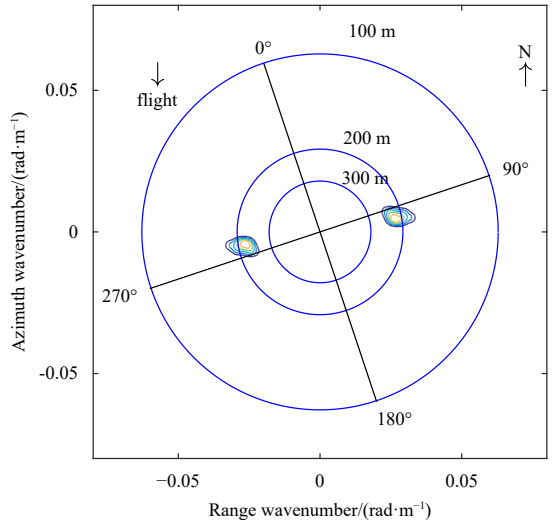


**Fig. 6.** Wave slope spectrum image obtained by CTLR mode of area south of Amchitkais, AK acquired by RADARSAT-2 at 05:47 UTC on February 28, 2009.

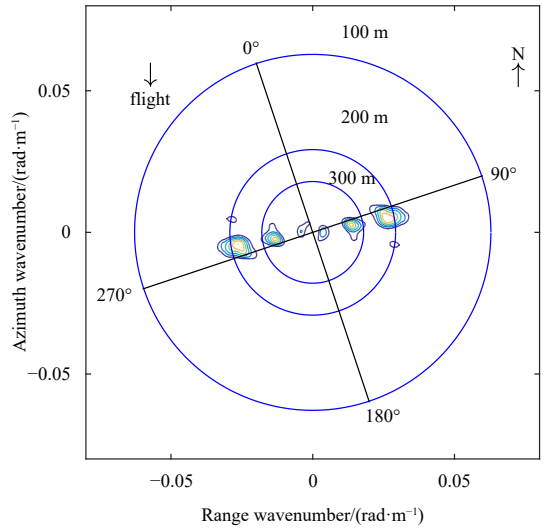


**Fig. 8.** Wave slope spectrum image obtained by π/4 mode of area south of Amchitkais, AK acquired by RADARSAT-2 at 05:47 UTC on February 28, 2009.

**Table 3.** The wave parameters of the four images in Table 2 are estimated and compared with the corresponding wave parameters of the NDBC buoys

| Parameter | Image | Buoy ID | Retrieval (CTLR) | Retrieval (π/4) | Buoy |
|---|---|---|---|---|---|
| Wave period/s | 1 | 46005 | 16.11 | 16.37 | 16.00 |
| | 2 | 46071 | 11.39 | 11.41 | 11.00 |
| | 3 | 46028 | 12.44 | 12.44 | 12.12 |
| | 4 | 46089 | 13.37 | 13.40 | 12.90 |
| Wavelength/m | 1 | 46005 | 405.4 | 418.9 | 399.5 |
| | 2 | 46071 | 202.7 | 203.3 | 188.8 |
| | 3 | 46028 | 241.7 | 241.7 | 229.2 |
| | 4 | 46089 | 279.3 | 280.5 | 259.7 |
| Wave direction/(°) | 1 | 46005 | 271.4 | 271.2 | 240.0 |
| | 2 | 46071 | 273.6 | 274.0 | 270.0 |
| | 3 | 46028 | 270.8 | 270.8 | 310.0 |
| | 4 | 46089 | 270.0 | 270.0 | 268.0 |

to be continued

Continued from Table 3

| Parameter | Image | Buoy ID | Retrieval (CTLR) | Retrieval (π/4) | Buoy |
|---|---|---|---|---|---|
| Significant wave height/m | 1 | 46005 | 3.44 | 3.31 | 3.10 |
| | 2 | 46071 | 3.21 | 3.81 | 4.10 |
| | 3 | 46028 | 3.02 | 3.02 | 2.88 |
| | 4 | 46089 | 2.03 | 2.58 | 2.51 |
| RMS slope/(°) | 1 | 46005 | 0.97 | 0.91 | 0.89 |
| | 2 | 46071 | 1.82 | 2.15 | 2.49 |
| | 3 | 46028 | 1.43 | 1.43 | 1.44 |
| | 4 | 46089 | 2.50 | 1.05 | 1.11 |

tion of the wave slope spectrum along the azimuth and range directions, it is not a complete wave slope spectrum. Hence, it cannot be converted into a wave spectrum for comparison with the spectrum derived from the buoy data.

## 5 Conclusions

In this paper, the effectiveness of the CTLR and π/4 models in retrieving the wave parameters is verified by directly using the c-band full-polarization SAR data and the CP SAR images obtained by using the compact polarization CTLR model and π/4 models, and the algorithm of wave parameters retrieval by using the polarization orientation angle and tilt modulation transfer function of the line-polarization SAR. The algorithm does not need complex hydrodynamics modulation function, and its wavelengths, wave heights, wave periods and wave propagation directions are consistent with these measured by buoys.

Since this experiment only studies the wave parameter retrieval algorithm for a single SAR image, the universality of CP SAR wave information inversion needs more experimental data to support. In future work, we plan to collect more fully polarimetric SAR data or directly use the CP SAR data provided by the RADARSAT Constellation Mission. In addition, we will evaluate other CP modes, such as dual circular polarization, for wave parameter retrieval. In addition, we intend to fuse the corresponding buoy data to improve the accuracy of retrieving wave parameters from CP SAR data.

## References

Ainsworth T L, Kelly J P, Lee J S. 2009. Classification comparisons between dual-pol, compact polarimetric and quad-pol SAR imagery. ISPRS Journal of Photogrammetry and Remote Sensing, 64(5): 464–471, doi: 10.1016/j.isprsjprs.2008.12.008

Charbonneau F J, Brisco B, Raney R K, et al. 2010. Compact polarimetry overview and applications assessment. Canadian Journal of Remote Sensing, 36(S2): S298–S315

Chen Lin, Cao F, Hong Wen. 2009. Unsupervised classification for compact polarimetric SAR data using m-δ decomposition, SPAN and the Wishart classifier. In: Proceedings of 2nd Asian-Pacific Conference on Synthetic Aperture Radar. Piscataway: IEEE, 742–745

Cloude S R, Goodenough D G, Chen H. 2012. Compact decomposition theory. IEEE Geoscience and Remote Sensing Letters, 9(1): 28–32, doi: 10.1109/LGRS.2011.2158983

Collins M J, Denbina M, Atteia G. 2013. On the reconstruction of Quad-Pol SAR data from compact polarimetry data for ocean target detection. IEEE Transactions on Geoscience and Remote Sensing, 51(1): 591–600, doi: 10.1109/TGRS.2012.2199760

Denbina M, Collins M J. 2012. Iceberg detection using compact polarimetric synthetic aperture radar. Atmosphere-Ocean, 50(4): 437–446, doi: 10.1080/07055900.2012.733307

Engen G, Johnsen H. 1995. SAR-ocean wave inversion using image cross spectra. IEEE Transactions on Geoscience and Remote Sensing, 33(4): 1047–1056 doi: 10.1109/36.406690

Fung A, Chan H L. 1969. Backscattering of waves by composite rough surfaces. IEEE Transactions on Antennas and Propagation, 17(5): 590–597, doi: 10.1109/TAP.1969.1139483

Guo Rui, Liu Yanbo, Wu Yirong, et al. 2012. Applying H/α decomposition to compact polarimetric SAR. IET Radar, Sonar & Navigation, 6(2): 61–70

Hasselmann S, Brüning C, Hasselmann K, et al. 1996. An improved algorithm for the retrieval of ocean wave spectra from synthetic aperture radar image spectra. Journal of Geophysical Research: Oceans, 101(C7): 16615–16629, doi: 10.1029/96JC00798

Hasselmann K, Hasselmann S. 1991. On the nonlinear mapping of an ocean wave spectrum into a synthetic aperture radar image spectrum and its inversion. Journal of Geophysical Research: Oceans, 96(C6): 10713–10729, doi: 10.1029/91JC00302

He Yijun. 1999. A parametric method of retrieving ocean wave spectra from synthetic aperture radar images. Chinese Science Bulletin, 44(13): 1218–1224, doi: 10.1007/BF02885970

He Yijun, Perrie W, Xie Tao, et al. 2004. Ocean wave spectra from a linear polarimetric SAR. IEEE Transactions on Geoscience and Remote Sensing, 42(11): 2623–2631, doi: 10.1109/TGRS.2004.836813

He Yijun, Shen Hui, Perrie W. 2006. Remote sensing of ocean waves by polarimetric SAR. Journal of Atmospheric and Oceanic Technology, 23(12): 1768–1773, doi: 10.1175/JTECH1948.1

He Yijun, Zhang Biao, Perrie W. 2009. Validation of RADARSAT-2 polarimetric SAR measurements of ocean waves. In: 2009 IEEE International Geoscience and Remote Sensing Symposium. Piscataway: IEEE, 3: III-168–III-171

Lee J S, Schuler D L, Ainsworth T L. 2000. Polarimetric SAR data compensation for terrain azimuth slope variation. IEEE Transactions on Geoscience and Remote Sensing, 38(5): 2153–2163, doi: 10.1109/36.868874

Lee J S, Schuler D L, Ainsworth T L, et al. 2002. On the estimation of radar polarization orientation shifts induced by terrain slopes. IEEE Transactions on Geoscience and Remote Sensing, 40(1): 30–41, doi: 10.1109/36.981347

Mastenbroek C, Valk C F D. 2000. A semiparametric algorithm to retrieve ocean wave spectra from synthetic aperture radar. Journal of Geophysical Research: Oceans, 105(C2): 3497–3516, doi: 10.1029/1999JC900282

Nord M E, Ainsworth T L, Lee J S, et al. 2009. Comparison of compact polarimetric synthetic aperture radar modes. IEEE Transactions on Geoscience and Remote Sensing, 47(1): 174–188, doi: 10.1109/TGRS.2008.2000925

Raney R K. 2006. Dual-polarized SAR and stokes parameters. IEEE Geoscience and Remote Sensing Letters, 3(3): 317–319, doi: 10.1109/LGRS.2006.871746

Raney R K. 2007. Hybrid-polarity SAR architecture. IEEE Transactions on Geoscience and Remote Sensing, 45(11): 3397–3404, doi: 10.1109/TGRS.2007.895883

Schuler D L, Jansen R W, Lee J S, et al. 2003. Polarisation orientation angle measurements of ocean internal waves and current fronts using polarimetric SAR. IEE Proceedings Radar, Sonar and Navigation, 150(3): 135–143

Schuler D L, Lee J S, Kasilingam D, et al. 2002. Surface roughness and slope measurements using polarimetric SAR data. IEEE Transactions on Geoscience and Remote Sensing, 40(3): 687–698,

doi: 10.1109/TGRS.2002.1000328

Schuler D L, Lee J S, Kasilingam D, et al. 2004. Measurement of ocean surface slopes and wave spectra using polarimetric SAR image data. Remote Sensing of Environment, 91(2): 198–211, doi: 10.1016/j.rse.2004.03.008

Shirvany R, Chabert M, Tourneret J Y. 2012. Ship and oil-spill detection using the degree of polarization in linear and hybrid/compact dual-pol SAR. IEEE Journal of Selected Topics in Applied Earth Observations and Remote Sensing, 5(3): 885–892, doi: 10.1109/JSTARS.2012.2182760

Souyris J C, Imbo P, Fjortoft R, et al. 2005. Compact polarimetry based on symmetry properties of geophysical media: the π/4 mode. IEEE Transactions on Geoscience and Remote Sensing, 43(3): 634–646, doi: 10.1109/TGRS.2004.842486

Souyris J C, Mingot S. 2002. Polarimetry based on one transmitting and two receiving polarizations: the π/4 mode. In: IEEE International Geoscience and Remote Sensing Symposium. Piscataway: IEEE, 629–631

Stacy N, Preiss M. 2006. Compact polarimetric analysis of X-band SAR data. In: Proceedings of the 6th European Conference on Synthetic Aperture Radar. Dresden, Germany: VDE Publishing House

Valenzuela G R. 1978. Theories for the interaction of electromagnetic and oceanic waves—a review. Boundary-Layer Meteorology, 13(1–4): 61–85, doi: 10.1007/BF00913863

Wang Xiaochen, Shao Yun, She Lu, et al. 2018. Ocean wave information retrieval using simulated compact polarized SAR from radarsat-2. Journal of Sensors, 2018: 1738014

Yin Junjun, Yang Jian, Zhang Xinzheng. 2011. On the ship detection performance with compact polarimetry. In: 2011 IEEE RadarCon (RADAR). Piscataway: IEEE, 2011: 675–680

Zhang Biao, Perrie W, He Yijun. 2010. Validation of RADARSAT-2 fully polarimetric SAR measurements of ocean surface waves. Journal of Geophysical Research: Oceans, 115(C6): C06031